Title

Altered iPSC-derived neurons' sodium channel properties in subjects with Monge's disease

Authors

Zhao, HW
Gu, XQ
Chailangkarn, T
et al.

Publication Date

2015-03-01

DOI

10.1016/j.neuroscience.2014.12.039

Peer reviewed

Published in final edited form as:
Neuroscience. 2015 March 12; 288: 187–199. doi:10.1016/j.neuroscience.2014.12.039.

Altered iPSC-derived neurons' sodium channel properties in subjects with Monge's disease

Huiwen W. Zhao[1], **Xiang Q. Gu**[1], **Thanathom Chailangkarn**[1,2], **Guy Perkins**[4], **David Callacondo**[5], **Otto Appenzeller**[6], **Orit Poulsen**[1], **Dan Zhou**[1], **Alysson R. Muotri**[1,2,7], and **Gabriel G. Haddad**[1,3,7,*]

[1]Department of Pediatrics, University of California San Diego, La Jolla, CA 92093

[2]Department of cellular and molecular medicine, University of California San Diego, La Jolla, CA 92093

[3]Department of Neurosciences, University of California San Diego, La Jolla, CA 92093

[4]National Center for Microscopy and Imaging Research, University of California San Diego, La Jolla, California, United States of America

[5]Laboratorios de Investigación y Desarrollo, Universidad Peruana Cayetano Heredia, Lima, Peru 36

[6]New Mexico Health Enhancement and Marathon Clinics Research Foundation, Albuquerque, NM 87122

[7]The Rady Children's Hospital, San Diego, CA 92123

Abstract

Monge's disease, also known as chronic mountain sickness (CMS), is a disease that potentially threatens more than 140 million highlanders during extended time living at a high altitude (over 2500m). The prevalence of CMS in Andeans is about 15-20%, suggesting that the majority of highlanders (non-CMS) are rather healthy at the high altitude; however, CMS subjects experience severe hypoxemia, erythrocytosis and many neurologic manifestations including migraine, headache, mental fatigue, confusion, and memory loss. The underlying mechanisms of CMS neuropathology are not well understood and no ideal treatment is available to prevent or cure CMS, except for phlebotomy. In the current study, we reprogrammed fibroblast cells from both CMS and non-CMS subjects' skin biopsies into the induced pluripotent stem cells (iPSCs), then differentiated into neurons and compared their neuronal properties. We discovered that CMS neurons were much less excitable (higher rheobase) than non-CMS neurons. This decreased excitability was not caused by differences in passive neuronal properties, but instead by a

[*]**Corresponding Author:** Gabriel G. Haddad, MD 9500 Gilman Drive, La Jolla, CA 92093-0735 Phone: 858-822-4740 Fax: 858-534-6972 ghaddad@ucsd.edu.

The authors declare no competing financial interests.

significantly lowered Na^+ channel current density and by a shift of the voltage-conductance curve in the depolarization direction. Our findings provide, for the first time, evidence of a neuronal abnormality in CMS subjects as compared to non-CMS subjects, hoping that such studies can pave the way to a better understanding of the neuropathology in CMS.

Keywords

chronic mountain sickness; induced pluripotent stem cells; neurons; Na^+ channel

Introduction

Chronic mountain sickness (CMS), also known as Monge's disease, was first described in 1925 by Carlos Monge. CMS is a disease that develops after an extended sojourn at high altitude, where highlanders are exposed to extreme hypobaric hypoxia as compared to lowlanders. In Andeans, the prevalence of CMS is about 15-20%, demonstrating that the majority of highlanders are rather healthy at the high altitude; in contrast, CMS subjects experience severe hypoxemia, excessive erythrocytosis and a panel of neuropathological symptoms including migraine, headache, mental fatigue, confusion, and memory loss (Monge, 1942, 1953). At high altitude, CMS subjects not only have difficulty in daily activities but also they suffer from increased mortality and morbidity due to moderate or severe pulmonary hypertension, cardiac pathology and stroke (Jha et al., 2002, Leon-Velarde, 2003, Leon-Velarde et al., 2010). Therefore, many researchers believe that CMS is a disease of “maladaptation” to high altitude. Currently, there is no ideal treatment available to prevent or cure CMS, except for phlebotomy (Richalet et al., 2005, Rivera-Ch et al., 2007, Rivera-Ch et al., 2008), and CMS has been classified as one of the global public health concerns that potentially threatens more than 140 million people living at high altitude (over 2500m) (Pasha and Newman, 2010).

Although hypobaric hypoxia at high altitude has been shown to cause structural and functional changes in human brain, such as neuropsychological changes and memory loss (Cavaletti et al., 1987a, Cavaletti and Tredici, 1993, Jeong et al., 2002, Hota et al., 2008, Dickinson et al., 2014), non-CMS subjects have a normal physical life without any evidence of neuropathological symptoms. Therefore, we hypothesize that CMS subjects may exhibit abnormal neuronal properties as compared to non-CMS subjects. Although previous studies have demonstrated that genetic causes play an important role in CMS subjects (Buroker et al., 2012a, b, 2013, Zhou et al., 2013), studies of CMS neuropathology, especially at the cellular level, have not been done. In the current study, we have used induced pluripotent stem cells (iPSCs) to generate neurons from non-CMS and CMS subjects’ fibroblast cells; we then compared the neuronal properties between the two groups, in the hope that such studies shed light on the function of neurons in both populations. This is the first step in investigating the underlying mechanisms of CMS susceptibility and their neurologic manifestations in humans.

Experimental procedures

Preparation of dermal fibroblasts from human skin biopsies

All subjects in the current study were adult males residing in the Andean mountain range, in Cerro de Pasco, Peru, at an elevation of more than 4,300 m. CMS subjects fulfilled the diagnostic criteria for CMS, or Monge disease based on their hematocrit, O_2 saturation and CMS score (> 12). Those with CMS score < 7 were chosen as non-CMS subjects (Table 1). Each subject signed an informed written consent under protocols approved by the University of California San Diego and the Universidad Peruana Cayetano Heredia.

Three mm skin punch biopsy samples were obtained from male highlanders with CMS (n = 3) and without CMS (n = 3) in Cerro de Pasco, Peru. The skin biopsies were mechanically dissociated and plated for dermal fibroblast expansion in DMEM medium supplement with 20% fetal calf serum, 2.5% penicillin/streptomycin and 1% fungizone antibiotic (Life technologies, CA). Fibroblasts grew from explants after 2-3 weeks and were passaged when they achieved 80% confluence.

Reprogramming of human fibroblast cells and generation of induced pluripotent stem cells (iPSCs)

Retrovirus vectors containing the Yamanaka factors (*OCT4*, *SOX2*, *KLF4* and *c-MYC* human cDNAs) (Takahashi et al., 2007) were manufactured by Salk Institute Gene Transfer, Targeting and Therapeutics Core (La Jolla, CA). Fibroblast cells were infected followed by two one-hour SpinFection protocol. The infected fibroblast cells were plated onto the irradiated mouse embryonic fibroblast feeder cells 24 hrs later with human embryonic stem cell medium containing 20% knockout serum replacement, 1% non-essential amino acids, 0.2% beta-mercaptoethanol, and 30ng/ml FGF2 in DMEM/F12 medium. Valproic acid (Sigma, MO) was added at day 5-9. Three weeks after SpinFection, compact colonies containing iPSC colonies appeared and were mechanically picked, transferred to a matrigel-coated dish (BD Bioscience, CA) and expended in mTeSR™ medium (StemCell Technologies, Canada). Three clones were picked from each individual and clone #3 from each subject was used for further differentiation and characterizations.

Generation of neural progenitor cells and induced neuronal differentiation

To obtain neural progenitor cells (NPCs), embryoid bodies (EBs) were formed following an EB spin protocol (Kim et al., 2011) with minor modifications. In brief, iPSCs were pretreated with 5μM Y-27632 (Stemgent, CA) one hour before detachment with accutase, iPSCs were triturated to single cells after resuspension in N2 medium containing 0.5x N2, 0.5x B27, 1% penicillin/streptomycin in DMEM/F12 medium plus 5μM Y-27632, 1μM dorsomorphin, 10 μM SB431542 (Tocris Bioscience, MN). Then an AggreWell plate (Stem Cell Technologies, Canada) was used to generate EBs following the manufacturer's instruction. At day 2, EBs were lifted and transferred to an ultra low attachment petri dish for another day using the same medium as above. At day 3, EBs were transferred to a matrigel-coated plate and cultured using N2 medium. After 7-10 days, rosettes were visible and rosette-bearing EBs were manually removed and dissociated into individual cells using accutase, and dissociated cells were then plated into a poly-L-ornithine/laminin coated plate

to generate a monolayer of NPC culture with N2 medium plus 20 ng/μl FGF2. To obtain neurons, the earlier passage (< passage 10) of NPCs was used to induce neuronal differentiation by withdrawing FGF2 from N2 medium (Shi et al., 2012).

DNA fingerprinting and high-resolution of Karyotyping

DNA was extracted from fibroblasts and iPSCs lines using a DNase blood and Tissue Kit (Qiagen, CA). DNA fingerprinting analysis and stem array, a high-resolution karyotyping, were performed by the Cell Line Genetics (Madison, WI).

Alkaline phosphatase staining and immunocytochemistry

The iPSCs were fixed with 4% paraformaldehyde for 20 min and alkaline phosphatase staining was performed using a Stemgent® Alkaline Phosphatase Staining Kit (Stemgent, CA) following the manufacturer's protocol. For immunocytochemistry, iPSCs, rosette, and neurons were fixed with 4% paraformaldehyde followed by blocking with 10% normal goat serum in PBST for 1 hour. Cells were then incubated with the appropriate primary antibodies against NANOG (1:500), TRA-1-81 (1:100), PAX6 (1:100, Stemgent), SOX1 (1:1000, BD Biosciences), MAP2 (1:1000, Sigma), TUJ-1 (1:1000, Covance), and VGLUT1 (1:5000, Syanptic System) overnight at 4°C and followed by proper FITC 488- or Alexa Fluor 568-labeled secondary antibodies (Molecular Probes, CA) for 1 hour. Antifade mounting medium with DAPI (Life Technologies, CA) was used for nuclear counterstaining. Fluorescent signals were detected using a Zeiss inverted Axiovert 200M microscope. Co-localizations of $MAP2^+$ and $DAPI^+$ as well as $VGLUT1^+$ and $MAP2^+$ were determined on all three individuals from each group, and at least 150 cells per subject were counted and data were analyzed using Image J (Version 1.45s, NIH, USA).

Embroid body-mediated *in vitro* differentiation of iPSCs

As described by Takahashi et al. (Takahashi et al., 2007), EBs were prepared as above without adding dorsomorphin and SB431542 and EBs were expended on the matrigel coated plates (BD Bioscience, CA) for additional 7 days. Then all cells were harvested for validating the *in vitro* differentiation using RT –PCR.

Reverse transcriptase PCR and genomic PCR

Total RNA from iPSCs (n = 6), human embryonic stem (ES) cell line H9 (a generous gift from Dr. Alysson Muotri, UCSD), EBs, fibroblasts, retrovirus-infected fibroblasts and neurons was extracted using the RNase Mini kit (Qiagen, CA). After removing genomic DNA with DNase I digestion (Ambion, TX), 1 μg of total RNA was converted to complementary of DNA using SuperScript First-Strand Synthesis System for RT-PCR (Life Technologies, CA). DNA from iPSCs and fibroblast cells was extracted using a DNase blood and tissue Kit (Qiagen, CA). Semi-quantitative PCR was performed on either complementary DNA or genomic DNA using Taq DNA polymerase (Life Technologies, CA) and real time PCR was then performed using POWER SYBR Green chemistry (Applied Biosystems, CA). Gene expression of *GAPDH* levels was used a loading control. H9 cells and retrovirus-infected fibroblasts were used as positive control and fibroblasts alone were used as negative control. Real time PCR data were presented after normalization

as a percentage of the non-CMS control. Primer sequences used in the current study was listed in table 2.

Immunoblotting

Neurons were homogenized with a glass-teflon homogenizer (Thomas Scientific, NJ) in RIPA buffer plus protease and phosphatase inhibitors (1 mM phenylmethylsulfonyl fluoride, 1 mM sodium orthovanadate, 10 μg/ml leupeptin, 1 μg/ml aprotinin, and 1 μg/ml antipain). Homogenates were then centrifuged for 10 min at 10,000 g and 4°C. The supernatants were collected and protein concentration was determined using a Bio-Rad protein assay kit (Bio-Rad, CA). Twenty micrograms of protein was separated on NuPAGE 4-12% Novex Bis-Tris gels and then transferred to polyvinylidene difluoride membranes (Millipore, CA). The membranes were probed with pan-Na channel antibody (1:1000, Alomone Labs, Israel) in PBST overnight at 4 °C and followed by a horseradish peroxidase-conjugated secondary antibody (anti-rabbit IgG, 1:10000, Zymed Laboratories, CA). Immunoreactive bands were visualized using Bio-Rad ChemiDoc XRS with enhanced chemiluminescence (Perkin-Elmer, MA). Equal loading was assessed using actin antibody (1:750, Santa Cruz Biotechnology, CA) and data were analyzed using ImageLab software (version 3.0, Bio-Rad, CA).

Dendrite size measurements

Electron microscope images taken at 1100 magnification were used to measure the width of dendrites. Proximal dendrite diameters were determined by measuring their width perpendicular to a line drawn from the center of the dendritic shaft to the nucleus that was the same distance to the edge of the nucleus for each cell measured. A total of 11 images were used for each group.

Whole-cell electrophysiology recordings

Electrodes for whole cell recording were pulled on a Flaming/Brown micropipette puller (Model P-87, Sutter Instrument, CA) from filamented borosilicate capillary glass (1.2 mm OD, 0.69 mm ID, World Precision Instruments, FL). The electrodes were fire-polished, and resistances were typically 2–5 MΩ for voltage-clamp experiments and 7–9 MΩ for current-clamp experiments. Before experiments, the N2 media were removed from the neuronal culture dish and replaced with a bath solution comprised of (in mM): 130 NaCl, 3 KCl, 1 $CaCl_2$, 1 $MgCl_2$, 10 HEPES, and 10 glucose (pH 7.4). The pipette solution contained (in mM): 138 KCl, 0.2 $CaCl_2$, 1 $MgCl_2$, 10 HEPES (Na^+ salt), and 10 EGTA, (pH 7.4). The osmolarity of all solutions was adjusted to 290 mOsm. All recordings were performed at room temperature (22-24°C). All chemicals were purchased from Sigma-Aldrich except $MgCl_2$ (J.T. Baker, PA). In some experiments, pharmacological ion channel antagonists were bath applied: Na^+ channels were blocked by tetrodotoxin (TTX, 2 μM).

The tested neurons (89 neurons from non-CMS and 42 from CMS) were obtained from all three individual subjects of each group. Neurons were selected for recording if they had a smooth surface and a three-dimensional contour; and if the patch seal resistance was > 1 GΩ, the holding current was < 0.1 nA (at a command potential of -80 mV), and the series resistance was < 10 MΩ. The series resistances were compensated at 90% level with the

Axopatch 1C amplifier (Molecular Devices, CA), and under these conditions, the error caused by uncompensated series resistances was < 0.1 mV. This error was not corrected. To obtain adequate voltage clamp and minimize space-clamp issues, only small neurons with short processes were used in our experiments. Membrane potential (V_m) was recorded in the current-clamp mode with zero current. Input resistance (R_m) was calculated in the current clamp mode by dividing the evoked voltage by a command current. Current traces in voltage clamp were leak-subtracted. Liquid junction potentials were nulled for each individual cell with the Axopatch 1C amplifier. Whole cell capacitance was assessed when capacitance transients were nulled in the whole cell configuration. Rheobases were assessed as the minimum injected current required to evoke an action potential in the current clamp mode. Na^+ currents were determined by injecting voltage in voltage steps of 10 mV between the range of −70 mV to 80 mV.

Statistics

All experiments were repeated at least twice and data were collected from three individuals in each group. Immunocytochemistry and electrophysiological data were analyzed using student t-test or one-way ANOVA and graphed using Origin 3.78 (OriginLab, MA) or GraphPad Prism 4.02 (GraphPad Software, Inc., CA). Results were expressed as group mean ± SEM. Difference in means were considered statistically significant when $p < 0.05$.

Results

Generation of iPSCs from non-CMS and CMS subjects

Fibroblast cells were generated from skin biopsies that were obtained from high altitude male, non-CMS (n = 3) and CMS (n = 3) subjects respectively. The hematocrit, O_2 saturation and CMS score of these individuals were listed in table 1. To generate iPSCs, fibroblast cells were transfected with retroviral reprogramming factors (*OCT4*, *SOX2*, *KLF4*, and *c-MYC*). Three weeks after transduction, compact iPSC colonies appeared, which were similar to human ES cells and characterized by large nuclei and scant cytoplasm. The iPSCs colonies were manually picked and cultured on the matrigel-coated plates for expansion (Fig. 1). A total of three clones were collected from each individual and one clone was used for further characterization and neural differentiation. DNA fingerprinting analysis of short tandem repeat confirmed that the obtained iPSCs line was identical to their parental somatic cell lines. Stem array, a higher resolution of karyotyping, confirmed that all iPSC colonies had a normal karyotype (Fig. 3A). In addition, to validate that the iPSCs lines were fully reprogrammed, the following evidence was provided, including 1) positive staining for pluripotency markers including NANOG and Tumor-related antigen (TRA)-1-81 (Fig. 2A), 2) positive staining for alkaline phosphatase (Fig. 3B), 3) similar expression of prominent endogenous pluripotency genes such as *OCT4*, *SOX2*, *c-MYC*, *KLF4*, *NANOG*, and *LIN28* was observed in iPSCs and H9 cells (Fig. 3C), 4) *in vitro* embryoid body-mediated differentiation with expression of multi-lineage differentiation markers including ectodermal markers (microtubule-associated protein 2/*MAP2* and paired box 6/*PAX6*), mesodermal markers (Msh homeobox1/*MSX1* and -smooth muscle actin /α-*SMA*), and endodermal markers (cytokeratin 8/*CK8* and cytokeratin 18/*CK18*) (Fig. 3D), and last, 5) presence of exogenous reprogramming factors in the genomic DNA of iPSCs (Fig. 3E), but the

expression of transgenes in the mRNA of iPSCs was low or undetectable (Fig.3F). These data suggested that iPSCs were pluripotent and have ability to differentiate into three germ layers *in vitro*.

Generation of neural progenitor cells and induced neuronal differentiation

To generate NPCs, we first used an AggreWell to form free-floating spheres following an EB spin protocol. EBs were then seeded onto matrigel coated plates and NPCs-containing rosettes appeared after 7-10 days (Fig. 1E & F). At this stage, rosettes were confirmed to be positive labeled for neural progenitor markers such as PAX6 and SOX1 (Fig. 2B) and were then manually picked and dissociated; a monolayer of NPCs was then seeded into poly-ornithine/laminin coated plates (Fig. 1G). Neural differentiation was initiated by withdrawing FGF2 when cells reached about 70% confluency (Marchetto et al., 2010, Shi et al., 2012). Neuronal morphology started to appear about ten days after differentiation (Fig. 1H). Three weeks after withdrawing FGF2, neurons that were positively labeled for neuronal markers such as MAP2 and TUJ1 started to be detected (Fig, 2C).

As described by Shi and his colleagues (Shi et al., 2012), the current neural differentiation protocol was used for cortical neurogenesis, the majority of neurons were glutamatergic neurons and the GABAergic interneurons were not generated under the cortical induction conditions unless specific factors were added. Similarly, we did not detect positive staining of GABA antibody in our neuronal cultures using immunocytochemistry. To characterizing the neuronal subpopulation in our iPSCs-derived neuronal cultures, we compared $MAP2^+$/$DAPI^+$ and $VGLUT1^+$/$MAP2^+$-stained neurons in the mixed cultures from both groups (Fig. 2D). The ratio of $MAP2^+$/$DAPI^+$ and $VGLUT1^+$/$MAP2^+$ neurons was not different between the two populations (Fig. 3G, $p > 0.05$) and most of the iPSCs-derived neurons using the current protocol were glutamatergic (> 90%) neurons. Real time PCR analysis further revealed a similar differentiation and developmental gene expression profiles in the neuronal cultures from both groups (Fig. 3H). This panel of genes includes *NES*, *SOX2* (for NPC), *MAP2*, *RBFOX3*, *TUBB3* (for neurons), *DLG4*, *SYN1* (for synapse), *GFAP*, *S100B* (for glia), *GABRR1*, *GAD1*, *SLC32A1* (for GABAergic neurons), *GRIA1*, *GRIN1*, *SLC17A7* (for glutamatergic neurons), *CUX2*, *FOXG1*, *RELN*, *STAB2*, and *TBR1* (for cortical layers).

Characterization of iPSCs-derived neurons using electrophysiology

To confirm that the differentiated neurons were functional and to study the properties of these neurons, we used the whole cell patch clamp. Around 25% of iPSCs-derived neurons fired action potentials spontaneously, but all neurons had evoked action potentials upon stimulation (Fig. 4A &B). These neurons had a rapid inward current and this current was not inhibited by bath application of 0.2 mM $CdCl_2$ but was eliminated completely by bath application of 2 μM TTX (Fig. 4C), indicating that these neurons possessed Na^+ currents.

Decreased excitability in CMS neurons—- In the current clamp mode, we observed that neurons derived from CMS subjects' fibroblasts had a significantly more depolarized action potential threshold than non-CMS neurons (Table 3, $p < 0.05$), and the minimum current (rheobase) required to evoke an action potential in CMS neurons (63.3 ± 9.1, from 41 neurons) was much higher than that in non-CMS neurons (25.1 ± 2.2 pA, from 88

neurons) (Fig. 4D, $p < 0.05$). In addition, the number of evoked action potentials during 162 ms command current for the CMS group was also significantly smaller than that in the non-CMS group (Table 3, $p < 0.05$), suggesting that the excitability of neurons derived from CMS subjects is much lower than that from non-CMS individuals.

To explore the reason(s) of the significantly different excitability between CMS and non-CMS neurons, we first measured the membrane passive properties, including resting membrane potential (V_m) and whole cell input resistance (R_m). No difference was found in V_m (−39.6 ± 2.0 mV for CMS and −39.6 ± 1.7 mV for non-CMS, $p > 0.05$) or R_m (2947 ± 432 M for CMS and 3450 ± 274 for non-CMS, $p > 0.05$), indicating that differences in passive membrane properties could not explain the lower excitability of CMS neurons. Using the whole cell patch clamp, we observed that the Na^+ currents from CMS neurons (216.9 ± 32.5 pA, from 42 neurons) were around 50% smaller than those from non-CMS neurons (392.1 ± 48.2 pA, from 89 neurons) (Fig. 5A & B, $p < 0.05$). This significant difference in the Na^+ current was still present when we normalized the Na^+ current to capacitance of the neurons (34.0 ± 6.0 pA/pF vs. 70.9 ± 8.3pA/pF) (Fig. 5C, $p < 0.05$).

Decreased Na^+ channel expression in CMS neurons—To determine whether a decreased Na^+ current density in CMS neurons is due to a decrease in Na^+ channel protein expression on the plasmalemma, we examined the abundance of Na^+ channel by a pan-Na channel antibody using western blotting. As expected, we found that CMS neurons had significantly less abundance of pan-Na^+ channel protein expression as evidenced by a decreased ratio of pan-Na^+/actin in the CMS group as compared to the non-CMS group (Fig. 5D & E, $p < 0.05$).

Previous studies have shown that neurons with thick dendrites tend to have high densities of Na^+ channels and those with thin dendrites have few or no dendritic Na^+ channels (Bischofberger and Jonas, 1997, Migliore and Shepherd, 2002). To examine whether dendritic size has effects on Na^+ channel density, we measured proximal dendrite diameters from neurons in each group and did not observe a significant difference in the dendritic width between two groups (1.87 ± 0.23 μm for non-CMS vs. 1.66 ± 0.23 μm for CMS, $p > 0.05$), suggesting that the decreased Na^+ density in CMS neurons was not caused by a decreased dendritic size.

Characterization of Na^+ current activation and inactivation—Whole cell Na^+ current at a particular voltage can be expressed as a product of a single channel amplitude, numbers of single channels in the whole cell, and single channel open probability. Whole cell equivalence of single channel open probability is a voltage conductance relationship or Na^+ channel activation curve. We then decided to test the activation characteristics of the Na^+ channel in the two populations of neurons. In the voltage clamp mode, we held the cell at -130 mV using a 48 ms command voltage from -70 to +80 mV with 10 mV increments and we obtained current curves at different voltages (Fig. 5A). We then plotted the normalized conductance against the membrane potentials and fit the points with Boltzmann equation. The mid-point of the voltage-conductance curve showed that there was a difference of 6.6 mV shift in the depolarization direction between the two groups (−23.4 mV for non-CMS vs. −16.8 mV for CMS) (Fig. 6A, $p < 0.05$). For example, at V_m = -30 mV,

G/G_{max} for the CMS neurons (0.09 ± 0.02) was significantly smaller than that for non-CMS neurons (0.30 ± 0.07). The slope factor was similar for CMS and non-CMS (6.71 vs. 6.25, $p > 0.05$).

Na^+ channel availability can be measured using a steady state inactivation curve. We used 500 ms prepulse potentials from −130 mV to −20 mV with increments of 10 mV and measured the peak currents at −20 mV (Fig. 6B). For both non-CMS and CMS neurons, if prepulses were between −130 and −80 mV, Na^+ currents were almost 100% available (Fig. 6C). When plotting the normalized current amplitudes vs. prepulse potentials, the relationship could be fit with a Boltzmann equation. The midpoint of steady state inactivation was −50.0 mV for non-CMS neurons and −48.7 mV for the CMS neurons ($p > 0.05$). The slope factors for both groups were 6.0 and 5.9 ($p > 0.05$) for non-CMS and CMS respectively.

Characterization of Na^+ current recovery from inactivation—Using variable durations between the two identical pulses of 25 ms at 0 mV from a holding voltage of −100 mV, we tested the characteristics of Na^+ current recovery from inactivation by measuring the ratio of current amplitudes of the second pulse over the first (Fig. 6D & E). Although there was no difference in the time constant of recovery (2.73 ms for non-CMS vs. 3.48 ms for CMS neurons, $p > 0.05$), when two pulses were 10.8, 13.6, 16.2 and 21.6 ms apart, recovery from inactivation was significantly slower in CMS neurons than that of non-CMS neurons (Fig 6E, $p < 0.05$).

Discussion

Since the iPSC technique was first introduced by Yamanaka (Takahashi et al., 2007), it has been rapidly used by many laboratories to study a variety of disease models in culture, such as Rett syndrome (Marchetto et al., 2010), Alzheimer's disease (Kondo et al., 2013), and Parkinson's disease (Hargus et al., 2010). Using a similar approach, we generated iPSCs from skin biopsies of non-CMS and CMS subjects and then differentiated them into different cell types, including neurons. The current study focuses on neurons because CMS subjects often experience migraine headache, mental fatigue, confusion, memory loss, as well as paresthesias, signs and symptoms that are believed to be caused by cerebral hypobaric hypoxia (Arregui et al., 1991, Arregui et al., 1994) and exacerbated by excessive erythrocytosis (Heinicke et al., 2006). In spite of the fact that hypobaric hypoxia (high altitude) has been shown to cause structural changes such as frontal subcortical and globus pallidus lesions as well as retinal hemorrhages(Cavaletti et al., 1987b, Jeong et al., 2002, Dickinson et al., 2014), and induce deleterious functional effects on the human brain (e.g., neural degeneration and memory loss) (Sorensen et al., 1974, Arregui et al., 1991, Cavaletti and Tredici, 1993, Jaillard et al., 1997, Hota et al., 2008), our understanding of CMS neuropathology at the cellular and molecular level is still limited. Indeed, to our knowledge, this study is the first to use iPSC-derived disease-specific human neurons as a model system to study the neuropathology of CMS.

Starting with skin biopsies obtained from non-CMS and CMS subjects, we were able to successively generate fibroblast cells, iPSCs, NPCs and then neurons without noticing any

major difference between two groups. All iPSCs lines have normal karyotyping and were fully reprogrammed from fibroblast cells, as evidenced by the absence of exogenous transcription factor expression but the presence of endogenous prominent pluripotency marker expression through either immunocytochemistry or RTPCR. The pluripotency of iPSCs were also confirmed by the alkaline phosphatase staining and embryoid body-mediated differentiation into three germ layers *in vitro*. The cells obtained from both populations had a similar morphology at all stages and a similar percentage of neural subtypes, suggesting that cells obtained from both groups have a similar reprogramming and differentiation ability, and characteristics that were not affected by the intrinsic differences as we have discovered here between the two groups.

As documented by Monge, CMS has an impressive familial character and is more frequent in men of European descent than men of any other genetic background in the Peruvian Andeans (Ergueta et al., 1971). The preferential ethnic backgrounds, familial character, and heritability of CMS suggested that genetic factors play an important role in the pathogenesis of CMS (Mejia et al., 2005, Moore et al., 2007). For instance, using SNP analysis, Buroke and others found that vascular endothelial growth factor (*VEGF*), v-akt murine thymoma viral oncogene homolog 3, Endothelial PAS domain-containing protein 1 and Egl nine homolog 1 SNPs were significantly associated with CMS pathology (Buroker et al., 2012a, b, 2013). Using whole genome sequencing, we have identified two genes, including sentrin specific peptidase 1(*SENP1***)** and Acidic leucine-rich nuclear phosphoprotein 32 family member D (*ANP32D*), out of eleven regions in the genome that have significant differences in haplotype frequencies between CMS and non-CMS (including the same subjects that were used for the current reprogramming studies). Real time PCR analysis confirmed that *SENP1* and *ANP32D* genes in CMS fibroblasts had a significantly higher transcriptional response under hypoxia as compared to that in non-CMS fibroblasts. Similar findings were also observed in neuronal cultures as well (Fig.7, $p < 0.05$). Decreased expression of *SENP1* and *ANP32D* orthologs in *Drosophila* also revealed an enhanced hypoxia tolerance in flies (Zhou et al., 2013), further providing evidence for the importance of these genes in hypoxia acclimatization. Interestingly, as reported by others, *SENP1* acts as a positive regulator of hypoxia-driven *VEGF* production and angiogenesis and was increased in endothelia cells under hypoxic conditions (Xu et al., 2010). Furthermore, decreased SUMOylation by overexpression of *SENP1* (as in CMS subjects) increases hippocampal neurons' vulnerability to oxygen-glucose deprivation-induced cell death (Cimarosti et al., 2012).

It is well known that sodium channels play an important role in axon development and neuronal circuit formation (Herrmann and Shatz, 1995, Zhang and Poo, 2001, Salthun-Lassalle et al., 2004, Uesaka et al., 2005, Black et al., 2006). Sodium channel abnormal expression and channelopathies can cause migraine headache (Frosk et al., 2013), poor memory performance (Dickinson et al., 2014), seizure, skeletal muscle paralysis, fatal cardiac arrhythmia, inflammatory pain, as well as neurodegeneration (Waxman, 2001, Wada, 2006), many of symptoms that are observed in CMS subjects. Our data showing that Na^+ current is decreased in CMS neurons as compared to non-CMS neurons, which lead us to believe that there is a causal link between CMS symptoms and sodium channel abnormalities and neuronal excitability. Modulations of ion channel properties have been

previously reported in response to hypoxia. For example, prolonged exposure to anoxia (Perez-Pinzon et al., 1993) or 10% O_2 (Xia and Haddad, 1999) decrease sodium channel abundance and density in neurons. However, since both CMS and non-CMS subjects have been living in the same hypoxic environments at high altitude for a prolonged period of time, and all our experiments were performed under the same room air conditions, the decreased Na^+ currents and current density observed in CMS neurons can be explained by either a different response to hypoxia by the CMS subjects or by an intrinsic difference between the two groups of neurons, likely to be genetic in nature.

The decreased Na^+ channel protein expression and altered properties are intriguing and are the major differences accounting for the decrease in excitability in CMS neurons. One might ask in light of these results whether these CMS neurons “benefit” from the decrease in excitability or is this decrease in excitability deleterious to these neurons? Is this decrease in excitability tantamount to an adaptive measure, possibly aimed at reducing the mismatch between cellular metabolic demand and O_2 supply and leading to an enhancement of neuronal survival? A decrease in energy consumption in the face of a decreased O_2/energy supply has been considered to be one of surviving strategies for long-term anoxia tolerance animals such as turtle, goldfish and *Drosophila* (Bickler et al., 2002, Wilkie et al., 2008, Zhou et al., 2008). In fact, we have demonstrated what genes and pathways are important for this survival in flies when deprived of O_2 (Zhou et al., 2008). Although CMS neurons have a decrease in neuronal excitability in comparison to non-CMS neurons, these individuals do not seem to be as well adapted to the hypoxic environment as the non-CMS neurons. Hence, there must be potentially other explanations and other mechanisms at play.

In summary, we used the iPSC technique to generate neurons from non-CMS and CMS subjects’ fibroblast cells and then used these subjects-specific neurons as a disease model to investigate the CMS neuropathology *in vitro*. We report that the excitability of CMS neurons was much lower than that of non-CMS neurons and further demonstrate that the decreased excitability was not caused by neuronal passive properties but instead, by a significant lowered Na^+ channel current density and abundance, in addition to alteration in Na^+ channel properties. Our data, for the first time provide evidence of dysfunction of sodium channels in CMS neurons and suggest that the decreased sodium channel expression and altered Na^+ channel properties might be one of the underlying mechanisms of CMS pathobiology.

Acknowledgments

This work was funded by the 5P01HL098053 from the National Heart, Lung, and Blood Institute to G.G.H. and funded by the 1-DP2-OD006495-01 from the National Institutes of Health through the NIH Director's New Innovator Award Program to A.M.. Authors also thank Pat Spindler for her generous help with the manuscript, Yu-Hsin Hisao and Ying Lu-Bo for their technical support.

Abbreviations

CMS	chronic mountain sickness
iPSCs	induced pluripotent stem cells

DMEM	Dulbecco's Modified Eagle Medium
NPCs	neural progenitor cells
EB	embryoid body
ES	embryonic stem
RIPA	Radioimmunoprecipitation assay buffer
TTX	tetrodotoxin
AP	Action potential
SUMO	Small Ubiquitin-like Modifier

References

Arregui A, Cabrera J, Leon-Velarde F, Paredes S, Viscarra D, Arbaiza D. High prevalence of migraine in a high-altitude population. Neurology. 1991; 41:1668–1669. [PubMed: 1922814]

Arregui A, Leon-Velarde F, Cabrera J, Paredes S, Vizcarra D, Umeres H. Migraine, polycythemia and chronic mountain sickness. Cephalalgia. 1994; 14:339–341. [PubMed: 7828191]

Bickler PE, Donohoe PH, Buck LT. Molecular adaptations for survival during anoxia: lessons from lower vertebrates. The Neuroscientist : a review journal bringing neurobiology, neurology and psychiatry. 2002; 8:234–242.

Bischofberger J, Jonas P. Action potential propagation into the presynaptic dendrites of rat mitral cells. The Journal of physiology. 1997; 504(Pt 2):359–365. [PubMed: 9365910]

Black JA, Waxman SG, Smith KJ. Remyelination of dorsal column axons by endogenous Schwann cells restores the normal pattern of Nav1.6 and Kv1.2 at nodes of Ranvier. Brain : a journal of neurology. 2006; 129:1319–1329. [PubMed: 16537565]

Buroker NE, Ning XH, Zhou ZN, Li K, Cen WJ, Wu XF, Zhu WZ, Scott CR, Chen SH. AKT3, ANGPTL4, eNOS3, and VEGFA associations with high altitude sickness in Han and Tibetan Chinese at the Qinghai-Tibetan Plateau. International journal of hematology. 2012a; 96:200–213. [PubMed: 22729570]

Buroker NE, Ning XH, Zhou ZN, Li K, Cen WJ, Wu XF, Zhu WZ, Scott CR, Chen SH. EPAS1 and EGLN1 associations with high altitude sickness in Han and Tibetan Chinese at the Qinghai-Tibetan Plateau. Blood cells, molecules & diseases. 2012b; 49:67–73.

Buroker NE, Ning XH, Zhou ZN, Li K, Cen WJ, Wu XF, Zhu WZ, Scott CR, Chen SH. VEGFA SNPs and transcriptional factor binding sites associated with high altitude sickness in Han and Tibetan Chinese at the Qinghai-Tibetan Plateau. The journal of physiological sciences : JPS. 2013; 63:183–193. [PubMed: 23553563]

Cavaletti G, Guazzi M, Marcucci A, Miani A, Petruccioli MG, Pizzini G, Tredici G, Viecca M. Endoneural vessel involvement in hypothyroidism. Italian journal of neurological sciences. 1987a; 8:259–264. [PubMed: 3623878]

Cavaletti G, Moroni R, Garavaglia P, Tredici G. Brain damage after high-altitude climbs without oxygen. Lancet. 1987b; 1:101. [PubMed: 2879152]

Cavaletti G, Tredici G. Long-lasting neuropsychological changes after a single high altitude climb. Acta neurologica Scandinavica. 1993; 87:103–105. [PubMed: 8442391]

Cimarosti H, Ashikaga E, Jaafari N, Dearden L, Rubin P, Wilkinson KA, Henley JM. Enhanced SUMOylation and SENP-1 protein levels following oxygen and glucose deprivation in neurones. Journal of cerebral blood flow and metabolism : official journal of the International Society of Cerebral Blood Flow and Metabolism. 2012; 32:17–22.

Dickinson D, Straub RE, Trampush JW, Gao Y, Feng N, Xie B, Shin JH, Lim HK, Ursini G, Bigos KL, Kolachana B, Hashimoto R, Takeda M, Baum GL, Rujescu D, Callicott JH, Hyde TM, Berman KF, Kleinman JE, Weinberger DR. Differential effects of common variants in SCN2A on

general cognitive ability, brain physiology, and messenger RNA expression in schizophrenia cases and control individuals. JAMA psychiatry. 2014; 71:647–656. [PubMed: 24718902]

Ergueta J, Spielvogel H, Cudkowicz L. Cardio-respiratory studies in chronic mountain sickness (Monge's syndrome). Respiration. 1971; 28:485–517. [PubMed: 5140341]

Frosk P, Mhanni AA, Rafay MF. SCN1A mutation associated with intractable myoclonic epilepsy and migraine headache. Journal of child neurology. 2013; 28:389–391. [PubMed: 22550089]

Hargus G, Cooper O, Deleidi M, Levy A, Lee K, Marlow E, Yow A, Soldner F, Hockemeyer D, Hallett PJ, Osborn T, Jaenisch R, Isacson O. Differentiated Parkinson patient-derived induced pluripotent stem cells grow in the adult rodent brain and reduce motor asymmetry in Parkinsonian rats. Proceedings of the National Academy of Sciences of the United States of America. 2010; 107:15921–15926. [PubMed: 20798034]

Heinicke K, Baum O, Ogunshola OO, Vogel J, Stallmach T, Wolfer DP, Keller S, Weber K, Wagner PD, Gassmann M, Djonov V. Excessive erythrocytosis in adult mice overexpressing erythropoietin leads to hepatic, renal, neuronal, and muscular degeneration. American journal of physiology Regulatory, integrative and comparative physiology. 2006; 291:R947–956.

Herrmann K, Shatz CJ. Blockade of action potential activity alters initial arborization of thalamic axons within cortical layer 4. Proceedings of the National Academy of Sciences of the United States of America. 1995; 92:11244–11248. [PubMed: 7479973]

Hota SK, Barhwal K, Singh SB, Ilavazhagan G. Chronic hypobaric hypoxia induced apoptosis in CA1 region of hippocampus: a possible role of NMDAR mediated p75NTR upregulation. Experimental neurology. 2008; 212:5–13. [PubMed: 18466900]

Jaillard AS, Mazetti P, Kala E. Prevalence of migraine and headache in a high-altitude town of Peru: a population-based study. Headache. 1997; 37:95–101. [PubMed: 9074294]

Jeong JH, Kwon JC, Chin J, Yoon SJ, Na DL. Globus pallidus lesions associated with high mountain climbing. Journal of Korean medical science. 2002; 17:861–863. [PubMed: 12483018]

Jha SK, Anand AC, Sharma V, Kumar N, Adya CM. Stroke at high altitude: Indian experience. High Alt Med Biol. 2002; 3:21–27. [PubMed: 12006161]

Kim JE, O'Sullivan ML, Sanchez CA, Hwang M, Israel MA, Brennand K, Deerinck TJ, Goldstein LS, Gage FH, Ellisman MH, Ghosh A. Investigating synapse formation and function using human pluripotent stem cell-derived neurons. Proceedings of the National Academy of Sciences of the United States of America. 2011; 108:3005–3010. [PubMed: 21278334]

Kondo T, Asai M, Tsukita K, Kutoku Y, Ohsawa Y, Sunada Y, Imamura K, Egawa N, Yahata N, Okita K, Takahashi K, Asaka I, Aoi T, Watanabe A, Watanabe K, Kadoya C, Nakano R, Watanabe D, Maruyama K, Hori O, Hibino S, Choshi T, Nakahata T, Hioki H, Kaneko T, Naitoh M, Yoshikawa K, Yamawaki S, Suzuki S, Hata R, Ueno S, Seki T, Kobayashi K, Toda T, Murakami K, Irie K, Klein WL, Mori H, Asada T, Takahashi R, Iwata N, Yamanaka S, Inoue H. Modeling Alzheimer's disease with iPSCs reveals stress phenotypes associated with intracellular Abeta and differential drug responsiveness. Cell stem cell. 2013; 12:487–496. [PubMed: 23434393]

Leon-Velarde F. Pursuing international recognition of chronic mountain sickness. High Alt Med Biol. 2003; 4:256–259. [PubMed: 12855057]

Leon-Velarde F, Villafuerte FC, Richalet J-P. Chronic mountain sickness and the heart. Prog Cardiovasc Dis. 2010; 52:540–549. [PubMed: 20417348]

Marchetto MC, Carromeu C, Acab A, Yu D, Yeo GW, Mu Y, Chen G, Gage FH, Muotri AR. A model for neural development and treatment of Rett syndrome using human induced pluripotent stem cells. Cell. 2010; 143:527–539. [PubMed: 21074045]

Mejia OM, Prchal JT, Leon-Velarde F, Hurtado A, Stockton DW. Genetic association analysis of chronic mountain sickness in an Andean high-altitude population. Haematologica. 2005; 90:13–19. [PubMed: 15642663]

Migliore M, Shepherd GM. Emerging rules for the distributions of active dendritic conductances. Nature reviews Neuroscience. 2002; 3:362–370.

Monge C. LIFE IN THE ANDES AND CHRONIC MOUNTAIN SICKNESS. Science. 1942; 95:79–84. [PubMed: 17757318]

Monge C. [Chronic mountain sickness in America]. El mal de montana cronico en America. An Fac Med Lima. 1953; 36:544–562. [PubMed: 13207756]

Moore LG, Niermeyer S, Vargas E. Does chronic mountain sickness (CMS) have perinatal origins? Respir Physiol Neurobiol. 2007; 158:180–189. [PubMed: 17706469]

Pasha MA, Newman JH. High-altitude disorders: pulmonary hypertension: pulmonary vascular disease: the global perspective. Chest. 2010; 137:13S–19S. [PubMed: 20522576]

Perez-Pinzon MA, Lutz PL, Sick TJ, Rosenthal M. Adenosine, a "retaliatory" metabolite, promotes anoxia tolerance in turtle brain. Journal of cerebral blood flow and metabolism : official journal of the International Society of Cerebral Blood Flow and Metabolism. 1993; 13:728–732.

Richalet JP, Rivera M, Bouchet P, Chirinos E, Onnen I, Petitjean O, Bienvenu A, Lasne F, Moutereau S, Leon-Velarde F. Acetazolamide: a treatment for chronic mountain sickness. Am J Respir Crit Care Med. 2005; 172:1427–1433. [PubMed: 16126936]

Rivera-Ch M, Huicho L, Bouchet P, Richalet JP, Leon-Velarde F. Effect of acetazolamide on ventilatory response in subjects with chronic mountain sickness. Respir Physiol Neurobiol. 2008; 162:184–189. [PubMed: 18603026]

Rivera-Ch M, Leon-Velarde F, Huicho L. Treatment of chronic mountain sickness: critical reappraisal of an old problem. Respir Physiol Neurobiol. 2007; 158:251–265. [PubMed: 17580125]

Salthun-Lassalle B, Hirsch EC, Wolfart J, Ruberg M, Michel PP. Rescue of mesencephalic dopaminergic neurons in culture by low-level stimulation of voltage-gated sodium channels. The Journal of neuroscience : the official journal of the Society for Neuroscience. 2004; 24:5922–5930. [PubMed: 15229240]

Shi Y, Kirwan P, Smith J, Robinson HP, Livesey FJ. Human cerebral cortex development from pluripotent stem cells to functional excitatory synapses. Nature neuroscience. 2012; 15:477–486. S471.

Sorensen SC, Lassen NA, Severinghaus JW, Coudert J, Zamora MP. Cerebral glucose metabolism and cerebral blood flow in high-altitude residents. J Appl Physiol. 1974; 37:305–310. [PubMed: 4412370]

Takahashi K, Tanabe K, Ohnuki M, Narita M, Ichisaka T, Tomoda K, Yamanaka S. Induction of pluripotent stem cells from adult human fibroblasts by defined factors. Cell. 2007; 131:861–872. [PubMed: 18035408]

Uesaka N, Hirai S, Maruyama T, Ruthazer ES, Yamamoto N. Activity dependence of cortical axon branch formation: a morphological and electrophysiological study using organotypic slice cultures. The Journal of neuroscience : the official journal of the Society for Neuroscience. 2005; 25:1–9. [PubMed: 15634761]

Wada A. Roles of voltage-dependent sodium channels in neuronal development, pain, and neurodegeneration. Journal of pharmacological sciences. 2006; 102:253–268. [PubMed: 17072104]

Waxman SG. Transcriptional channelopathies: an emerging class of disorders. Nature reviews Neuroscience. 2001; 2:652–659.

Wilkie MP, Pamenter ME, Alkabie S, Carapic D, Shin DS, Buck LT. Evidence of anoxia-induced channel arrest in the brain of the goldfish (Carassius auratus). Comparative biochemistry and physiology Toxicology & pharmacology : CBP. 2008; 148:355–362. [PubMed: 18620076]

Xia Y, Haddad GG. Effect of prolonged O2 deprivation on Na+ channels: differential regulation in adult versus fetal rat brain. Neuroscience. 1999; 94:1231–1243. [PubMed: 10625063]

Xu Y, Zuo Y, Zhang H, Kang X, Yue F, Yi Z, Liu M, Yeh ET, Chen G, Cheng J. Induction of SENP1 in endothelial cells contributes to hypoxia-driven VEGF expression and angiogenesis. The Journal of biological chemistry. 2010; 285:36682–36688. [PubMed: 20841360]

Zhang LI, Poo MM. Electrical activity and development of neural circuits. Nature neuroscience. 2001; 4(Suppl):1207–1214.

Zhou D, Udpa N, Ronen R, Stobdan T, Liang J, Appenzeller O, Zhao HW, Yin Y, Du Y, Guo L, Cao R, Wang Y, Jin X, Huang C, Jia W, Cao D, Guo G, Gamboa JL, Villafuerte F, Callacondo D, Xue J, Liu S, Frazer KA, Li Y, Bafna V, Haddad GG. Whole-genome sequencing uncovers the genetic basis of chronic mountain sickness in Andean highlanders. American journal of human genetics. 2013; 93:452–462. [PubMed: 23954164]

Zhou D, Xue J, Lai JC, Schork NJ, White KP, Haddad GG. Mechanisms underlying hypoxia tolerance in Drosophila melanogaster: hairy as a metabolic switch. PLoS genetics. 2008; 4:e1000221. [PubMed: 18927626]

Highlights

- iPSCs-derived neurons are generated from CMS and non-CMS subjects
- Neurons are characterized and neuronal properties are compared
- CMS neurons are much less excitable than non-CMS neurons
- The decreased excitability in CMS neurons is due to alteration in Na^+ channel properties

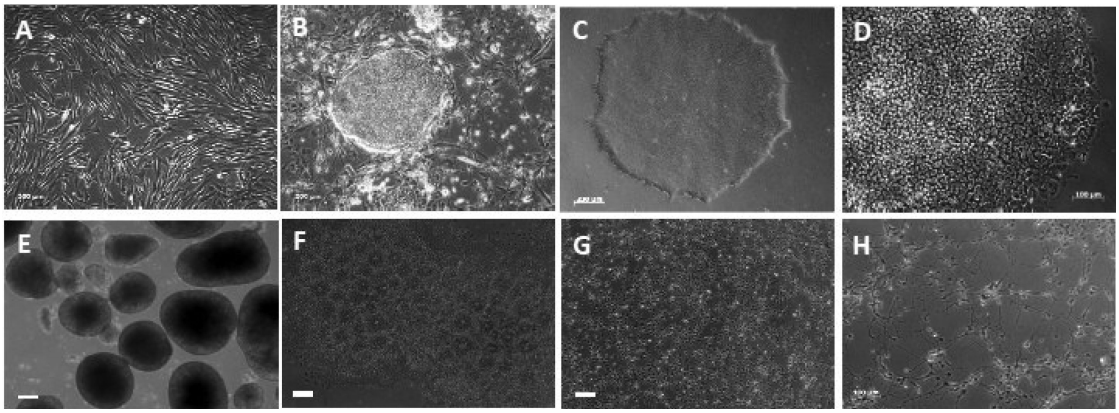

Figure 1. Generation of iPSCs-derived neurons from fibroblasts

A) Morphology of human fibroblasts obtained from skin biopsies. **B-D)** Formation of iPSC colonies through reprogramming processes. **E)** Formation of EBs from iPSCs and **F-G)** rosettes were picked to generate NPCs. **H)** Morphology of induced neurons from NPCs. Scale bar = 200 μm unless otherwise stated.

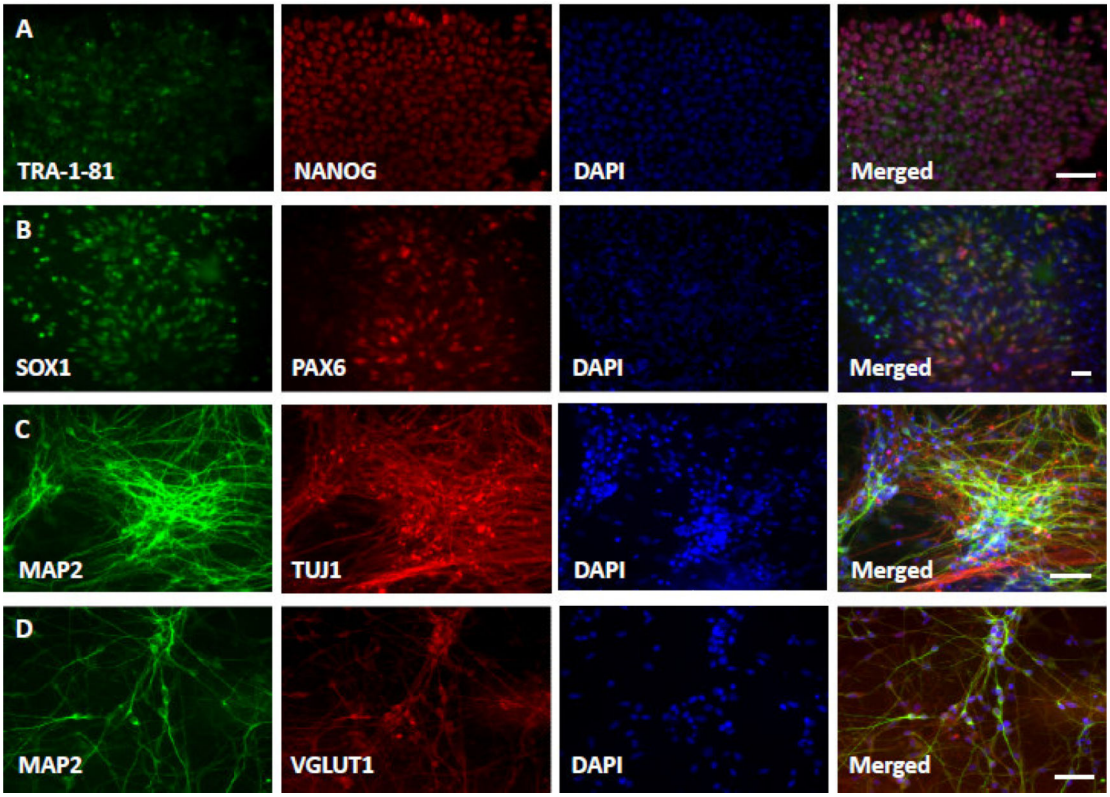

Figure 2. Characterization of iPSCs, NPCs and neurons

A) Representative images of iPSCs expressing pluripotency markers including NANOG and TRA-1-81. **B)** Rosettes expressing neural precursor markers including PAX6 and SOX1. **C)** iPSCs-derived neurons expressing neuronal markers including MAP2 and TUJ1. Scale bar for **A-C** = 200 μm. **D)** Representative images of iPSCs-derived neurons from CMS subjects expressing glutamatergic neuronal markers including MAP2 and VGLUT1, Scale bar = 50 μm.

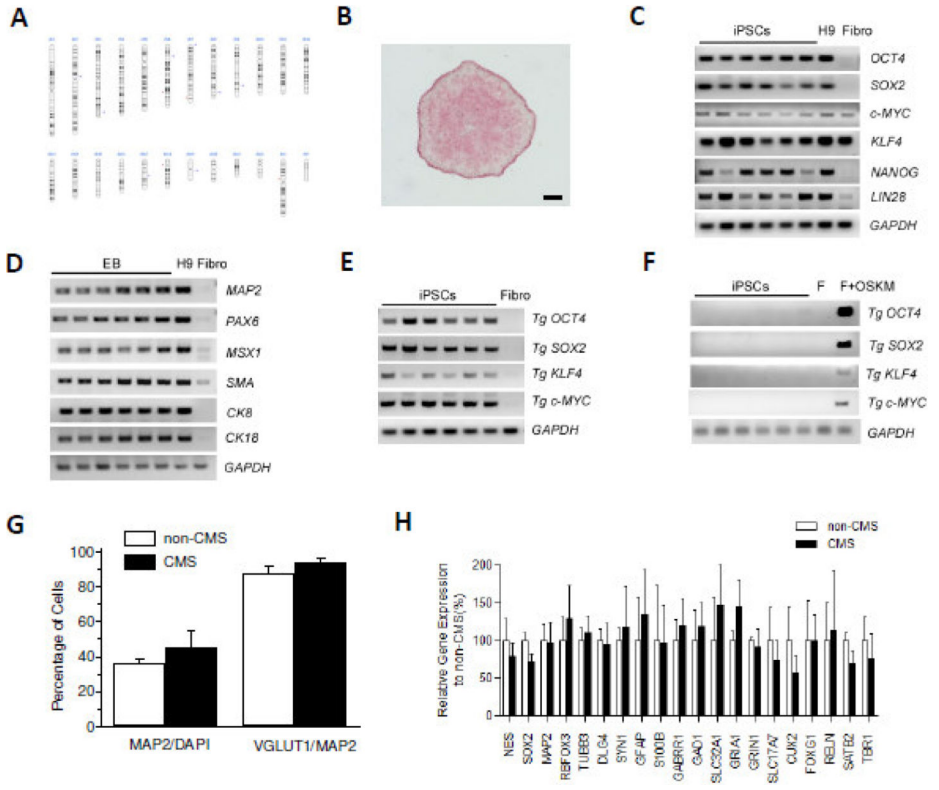

Figure 3. Characterization of iPSCs and neurons

A) No karyotypic abnormalities were observed in iPSC lines. **B)** Alkaline phosphatase staining of iPSCs. Scale bar = 200 μm. **C)** RT-PCR analysis of iPSC lines detected the transcripts of endogenous pluripotency embryonic stem cell markers. **D)** RT-PCR analysis of EBs detected the variety of differentiation markers for the three germ layers. **E)** Genomic RT-PCR revealed integration of all four retrovirus factors in iPSCs lines. **F)** The expression of transgenes was low or undetectable in the mRNA of iPSCs. Lane 1-6 was either iPSCs or EBs obtained from non-CMS (n = 3) and CMS (n = 3) subjects. Fibroblast cells (Fibro) were used as negative control, H9 cells and retrovirus-infected fibroblasts (F + OSKM) were used as positive control accordingly. **G)** Similar percentages of $MAP2^{+}/DAPI^{+}$ neurons and $VGLUT1^{+}/MAP2^{+}$ neurons observed in CMS and non-CMS neuronal populations. **H)** Similar neuronal differentiation and developmental stages between non-CMS and CMS neuronal cultures. Real time PCR results confirmed that neuronal cultures from both groups had a similar gene expression profile ($p > 0.05$).

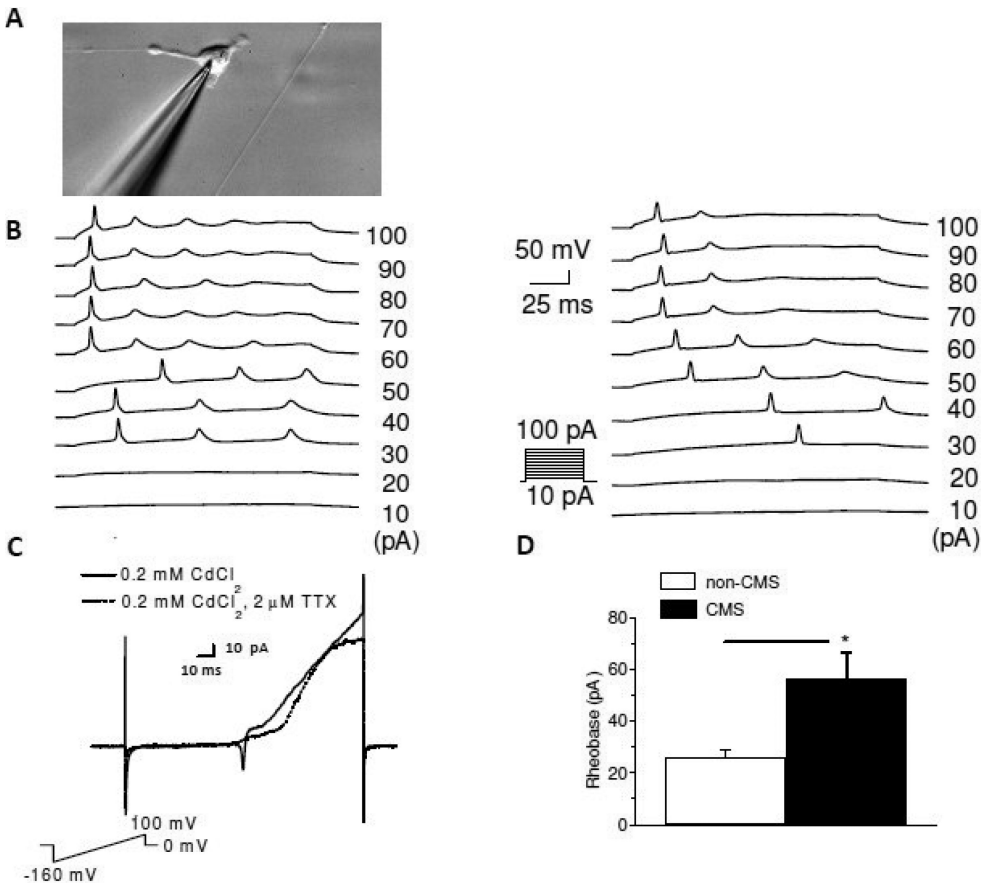

Figure 4. Characterization of action potentials from 33.7 days old non-CMS neurons and 32.8 days old CMS neurons after differentiation

A) A representative image of neurons from CMS neurons for patch clamping. **B**) Representative traces of evoked action potential from non-CMS (left) and CMS (right) neurons. **C)** 2 μM TTX completely eliminates the rapid inward current in neurons. **D)** CMS neurons (42) have a higher rheobase than non-CMS neurons (89). * indicates $p < 0.05$.

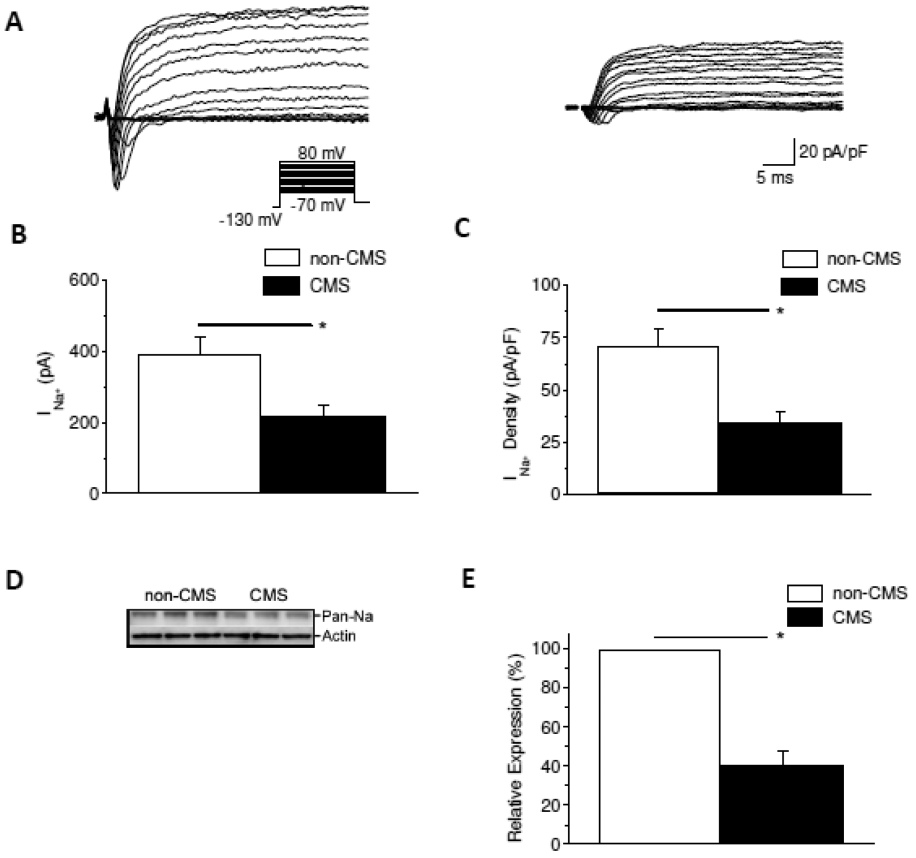

Figure 5. Decreased Na^+ currents, current densities and protein expression in CMS neurons

A) Representative Na^+ current traces from non-CMS (left) and CMS (right) neurons. **B)** Decreased Na^+ currents from non-CMS neurons (89) and CMS neurons (42), **C)** current densities and **E)** protein expression in CMS neurons. **D)** Representative immunoblots probed with anti-pan Na and -actin. * indicates $p < 0.05$.

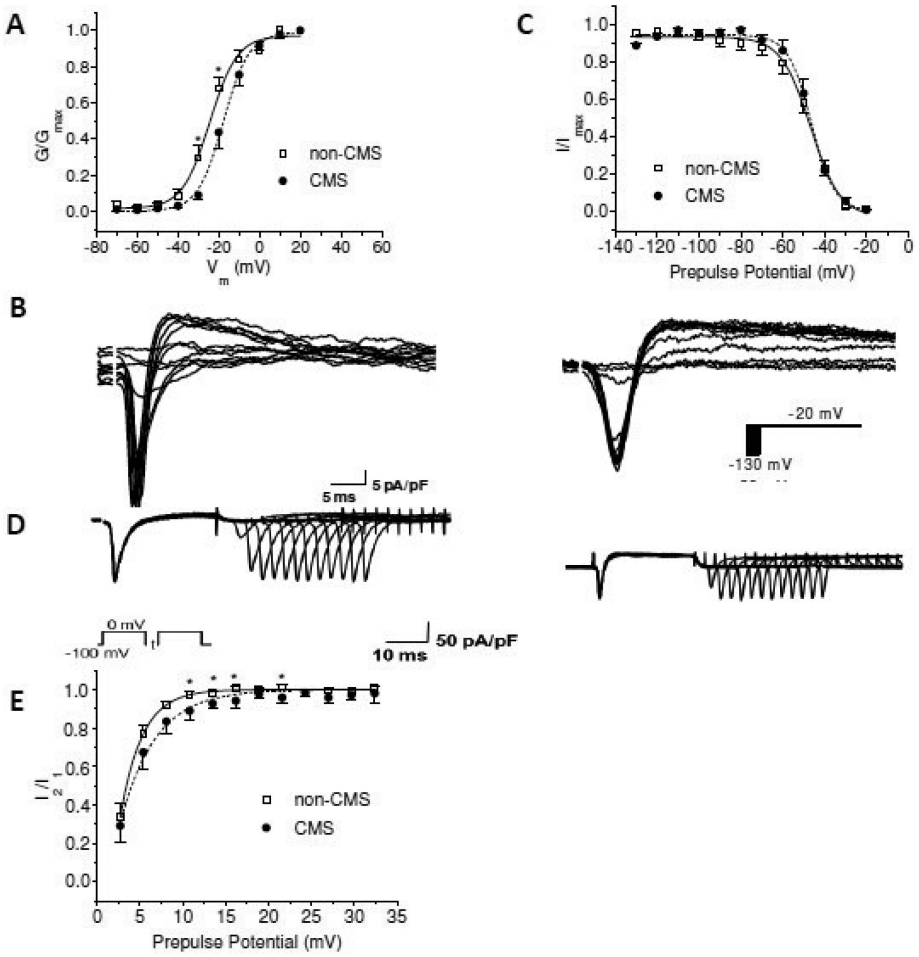

Figure 6. Na^+ current activation and inactivation

A) Activation of Na^+ currents from non-CMS neurons (29) and CMS neurons (15). **B)** Representative steady state inactivation of Na^+ currents from non-CMS (left) and CMS (right), data summarized in **C)**. **D)** Recovery from inactivation of Na^+ currents from non-CMS (left, 18) and CMS neurons (right, 10), data were summarized in **E)**. * indicates $p < 0.05$.

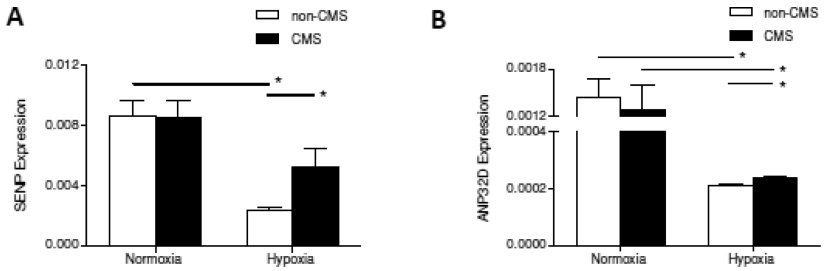

Figure 7. Gene expression profiles of *SENP1* and *ANP32D* in non-CMS and CMS neurons under normoxia and hypoxia

A) Real time PCR analysis confirmed that expression of *SENP1* was not different between non-CMS and CMS neurons under normoxia ($p > 0.05$), but there was a significantly different response between the two groups to 1% hypoxia treatment for 24 hrs ($p < 0.05$). Hypoxia treatment significantly decreased *SENP1* expression in non-CMS neurons as compared to that under normoxia ($p < 0.05$), but not in CMS neurons. **B)** Real time PCR analysis confirmed that expression of *ANP32D* was not different between non-CMS and CMS neurons under normoxia ($p > 0.05$), but there was a significantly different response between the two groups to 1% hypoxia treatment for 24 hrs ($p < 0.05$). Hypoxia treatment significantly decreased *ANP32D* expression in both non-CMS and CMS neurons as compared to that under normoxia ($p < 0.05$). * indicates $p < 0.05$.

Table 1

Summary of non-CMS and CMS subjects used in the current study as well as their medical test scores

Group	Subject ID	Age	Dizziness	Physical weakness	Mental fatigue	Anorexia	Muscle weakness	Joint pain	Breathlessness	Palpitations	Disturbed sleep	Cyanosis	Injected conjuncative	Dilation	Paresthesia	Headache	Tinnitus	Hct score	Sat score	Hct	Sat (%)	CMS score
non-CMS	10AL	33	1	0	0	0		0	0	0	2	2	0	2	0	0	0	0	0	51	85	7
	15EP	31	0	0	0	0	0	0	0	0	0	0	0	0	0	0	0	0	0	54	90	0
	24JR	23	0	0	0	0	0	0	0	0	0	0	0	0	0	3	0	0	0	52	90	3
CMS	16ES	22	0	0	0	0	0	0	2	2	2	2	2	0	2	3	3	3	0	65	85	21
	19JB	37	0	0	0	1	0	1	2	0	0	2	2	0	2	3	0	3	3	76	80	19
	33JM	34	0	0	1	0	1	0	0	0	2	2	0	0	2	3	3	3	0	63	83	17

Table 2

Primers used in the current study.

For RT-PCR		
	Forward	**Reverse**
Tg OCT4	CTGGCGGCAGCCTACCAAGA	GGCGAAATCCGAAGCCAGGT
Tg SOX2	CTGGCGGCAGCCTACCAAGA	GCGGGACCACACCATGAAGG
Tg KLF4	CTGGCGGCAGCCTACCAAGA	TCCTCCCGCCAGCGGTTATT
Tg c-MYC	CTGGCGGCAGCCTACCAAGA	GCAACGTAGGAGGGCGAGCA
OCT4	GACAGGGGGAGGGGAGGAGCTAGG	CTTCCCTCCAACCAGTTGCCCCAAAC
SOX2	GGGAAATGGGAGGGGTGCAAAAGAGG	TTGCGTGAGTGTGGATGGGATTGGTG
KLF4	AATAACCGCTGGCGGGAGGA	TCCAATTCTGGCCGCAGGAG
c-MYC	GCGTCCTGGGAAGGGAGATCCGGAGC	TTGAGGGGCATCGTCGCGGGAGGCTG
NANOG	GGCTGCCTTGGAAGCTGCTG	AACCCGGGAGACGGAGCTTG
LIN28	GACGACCATGGGCTCCGTGT	GGCCGCCTCTCACTCCCAAT
MAP2	CAGGTGGCGGACGTGTGAAAATTGAGAGTG	CACGCTGGATCTGCCTGGGGACTGTG
PAX6	ACCCATTATCCAGATGTGTTTGCCCGAG	ATGGTGAAGCTGGGCATAGGCGGCAG
MSX1	CGAGAGGACCCCGTGGATGCAGAG	GGCGGCCATCTTCAGCTTCTCCAG
SMA	CTGAGCGTGGCTATTCCTTC	GCTGGAAGGTGGACAGAGAG
CK8	CCTGGAAGGGCTGACCGACGAGATCAA	CTTCCCAGCCAGGCTCTGCAGCTCC
CK18	AGCTCAACGGGATCCTGCTGCACCTTG	CACTATCCGGCGGGTGGTGGTCTTTTG
GAPDH	GCACCGTCAAGGCTGAGAAC	CGCCCCACTTGATTTTGG

For real time PCR		
	Forward	**Reverse**
NES	GCTGCGGGCTACTGAAAA	CTGAGCGATCTGGCTCTGTA
SOX2	CATGAAGGAGCACCCGGATTA	CGGGCAGCGTGTACTTATCC
MAP2	CAACGGAGAGCTGACCTCA	CTACAGCCTCAGCAGTGACTA
RBFOX3	GAAGACGGGGAACCCCTACA	GCATAGAATTCAGGCCCGTAGAC
TUBB3	GAGCGGATCAGCGTCTACTA	GGTTCCAGGTCCACCAGAA
DLG4	AGCTGGAGCAGGAGTTCAC	ACACGCTTCACCTTGTGGTA
SYN1	GCAAGGACGGAAGGGATCA	TGTCTTCATCCTGGTGGTCAC
GFAP	GCCAGTTGCAGTCCTTGAC	GCGCATCTGCCTCTCCA
S100B	GGAGACAAGCACAAGCTGAA	CCATGACTTTGTCCACAACC
GABRR1	GCCTGATGGGAAAGTGCTCTA	TCCAAGGGAAATCGGCTGAA
GAD1	ATCCTGGTTGACTGCAGAGAC	CCAGTGGAGAGCTGGTTGAA
SLC32A1	AGGCTGGAACGTGACCAAC	GAGAAACAACCCCAGGTAGCC
GRIA1	CGCTCCACGTGATTGAAATGAA	TGGCTGCAGGGACAAACTTA
GRIN1	GGCAACACCAACATCTGGAA	CCATCCGCATACTTGGAAGAC
SLC17A7	GCCATCTCCTTCCTGGTCCTA	GGCTATGTCCAGGTGGTTCAC
CUX2	TCCATCACCAAGAGGGTGAA	CAGGATGCTTTCCCCAAACA

For real time PCR		
	Forward	**Reverse**
FOXG1	GCCAGCAGCACTTTGAGTTA	TGAGTCAACACGGAGCTGTA
RELN	TCCAGAATTGGAAGCGGATCA	GTTGGCCTGAATCCATCTGAAC
SATB2	TTTGCCAAAGTGGCTGCAAA	TTTCTGGGCTTGGGTTCTCC
TBR1	ACGAACAACAAAGGAGCTTCA	TGGTACTTGTGCAAGGACTGTA
GAPDH	GCACCGTCAAGGCTGAGAAC	CGCCCCACTTGATTTTGG

Table 3

Characteristics of evoked action potential.

	non-CMS	CMS
Delay (ms)	70.9±9.7	69.5±11.0
Threshold (-mV)	35.0±1.7	28.8±2.3 *
t to peak (ms)	3.1±0.2	2.9±0.2
½ Width (ms)	3.0±0.2	3.4±0.3
Amplitude (mV)	63.7±3.6	59.7±3.7
# of AP	2.1±0.2	1.4±0.1 *
n	25	20

* $p < 0.05$